GDCh Research Article Angewandte International Edition Chemie www.angewandte.org

How to cite: *Angew. Chem. Int. Ed.* **2025**, e202504630
doi.org/10.1002/anie.202504630

CO_2 Reduction | Very Important Paper

Using Host-Guest Chemistry to Examine the Effects of Porosity and Catalyst-Support Interactions on CO_2 Reduction

*Daniel A. Rothschild, Zeyu Cao, Feng Xie, Belvin Thomas, Thomas J. Emge, Jing Li, Tewodros Asefa, and Mark C. Lipke**

Abstract: Bis-porphyrin nanocages (**M_2BiCage**, M = FeCl, Co, Zn) and their host-guest complexes with C_{60} and C_{70} were used to examine how molecular porosity and interactions with carbon nanomaterials affect the CO_2 reduction activity of metalloporphyrin electrocatalysts. The cages were found to adsorb on carbon black to provide electrocatalytic inks with excellent accessibilities of the metal sites (≈50%) even at high metal loadings (2500 nmol cm^{-2}), enabling good activity for reducing CO_2 to CO. A complex of C_{70} bound inside **$(FeCl)_2$BiCage** achieves high current densities for CO formation at low overpotentials ($|j_{CO}|$ >7 mA cm^{-2}, η = 320 mV; >13.5 mA cm^{-2}, η = 520 mV) with ≥95% Faradaic efficiency (FE_{CO}), and **Co_2BiCage** achieves high turnover frequencies (≈1300 h^{-1}, η = 520 mV) with 90% FE_{CO}. In general, blocking the pore with C_{60} or C_{70} improves the catalytic performance of **$(FeCl)_2$BiCage** and has only small effects on **Co_2BiCage**, indicating that the good catalytic properties of the cages cannot be attributed to their internal pores. Neither enhanced electron transfer rates nor metal-fullerene interactions appear to underlie the ability of C_{60}/C_{70} to improve the performance of **$(FeCl)_2$BiCage**, in contrast to effects often proposed for other carbon nanosupports.

Introduction

Electrochemical CO_2 reduction (CO_2RR) is of interest for the renewable production of fuels and other chemicals.[1] To maximize the efficiencies of these emerging synthetic methods,[2,3] electrocatalysts are needed that can selectively carry out a specific transformation (e.g., CO_2 to CO conversion[4–6]) while minimizing the overpotential needed to achieve high turnover frequencies (TOF).[2,3,7,8] Considerable progress has been made in developing metalloporphyrin[9–14] (PorM) and metallophthalocyanine[15–17] (PcM) based molecular catalysts to achieve these goals, but heterogeneous catalysts are desired for practical implementation.[2,3,18–20] Thus, many efforts have been made over the past decade to attach PorM and PcM complexes to electrodes for use in CO_2RR.[21–24]

Scheme 1 illustrates two leading strategies for immobilizing these catalysts: 1) incorporating the PorM or PcM complexes into molecularly defined porous materials such as MOFs,[25–28] COFs,[29–40] and discrete nanocages;[41–44] or 2) adsorbing these complexes on conductive supports, such as carbon nanotubes (CNTs).[17,45–54] Both approaches have led to improved CO_2RR activity,[17,31–33,44,47,49,51] selectivity,[26,29,34,36,37,44,47–51] and overpotentials[26,45,46,49,50] relative to PorM and PcM catalysts in solution or deposited on electrodes using simpler methods. However, even for the most studied reactivity (CO formation), increases in current densities at low overpotentials would be needed to meaningfully improve upon traditional inorganic heterogeneous catalysts.[2,3] Achieving this goal is hindered by a lack of understanding of how different catalyst immobilization strategies affect activity.

Mechanistic conjectures regarding nanoporous catalysts are especially varied and contradictory.[55–58] For example, well-defined pores in MOFs, COFs, and other molecular materials are often claimed to benefit CO_2RR by increasing the accessibility of the catalytic metal sites,[25,27–29,32–34,41,43] but in many cases, only a low fraction of the metal centers (<10%)[26,29,31,37] are electrochemically addressable. Likewise, it is often suggested that the hydrophobic pores of these materials can promote the uptake of CO_2,[26,27,29,31–36,41,43,44,55,56] but the low relative permittivity of the confined active sites might also inhibit charge redistribution that occurs during CO_2 activation.[59,60] An analysis of these effects is confounded by the low conductivity of many MOFs and COFs,[61] which likely inhibits their CO_2RR activity.[62–67] Conversely, carbon nanotubes are used to provide efficient electron transport to adsorbed catalysts,[45–54] but like MOFs and COFs, these supports might also exert local influences on catalysis. For example, the curved nanotube surface may induce geometric distortions in PcM catalysts that alter their selectivity,[68] and the performance of PorM

[*] D. A. Rothschild, Z. Cao, F. Xie, B. Thomas, T. J. Emge, J. Li, T. Asefa, M. C. Lipke
Department of Chemistry and Chemical Biology, Rutgers The State University of New Jersey, 123 Bevier Rd, Piscataway, NJ 08854, USA
E-mail: ml1353@chem.rutgers.edu

Additional supporting information can be found online in the Supporting Information section

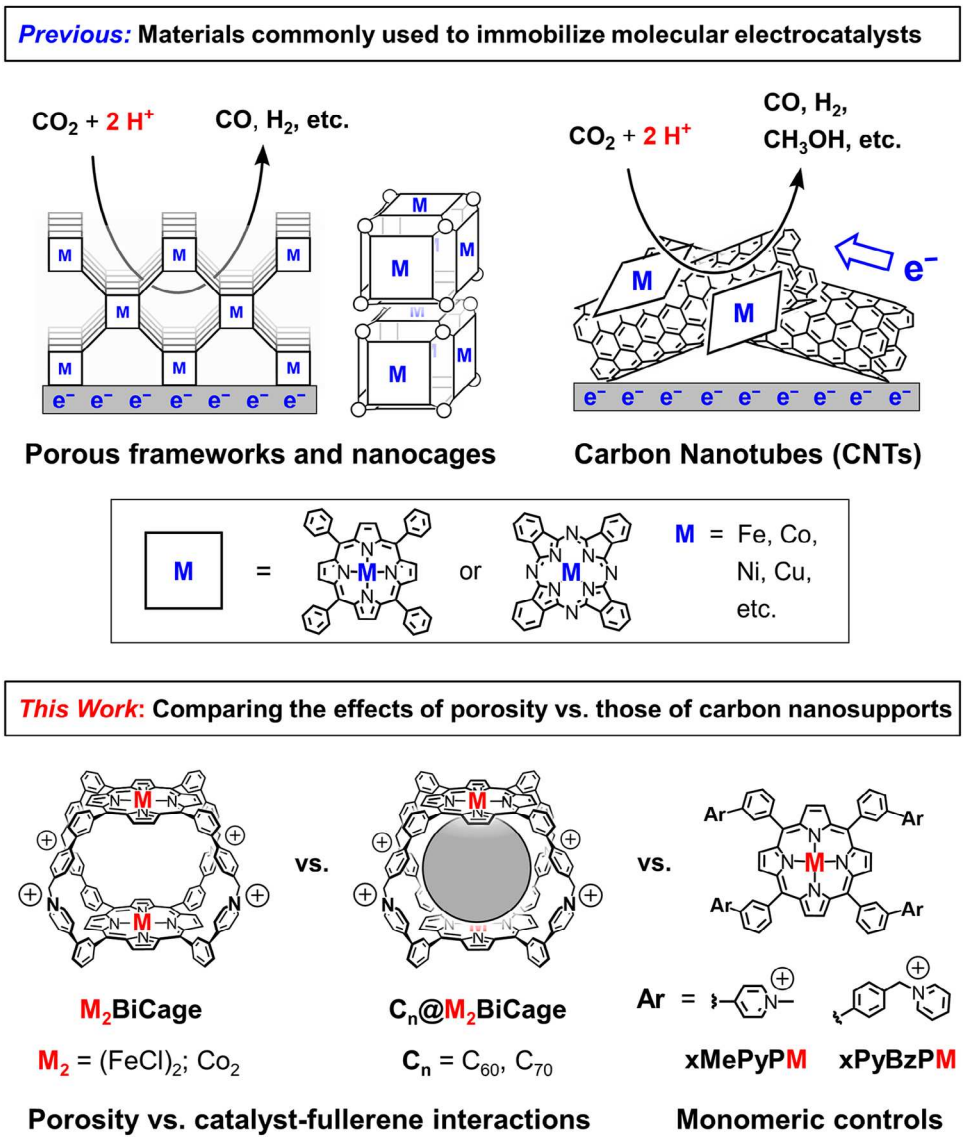

Scheme 1. (Top) Approaches for securing porphyrin and phthalocyanine complexes to electrodes for use as CO_2 reduction catalysts; (Bottom) Discrete nanocages for comparing the local effects of porosity and catalyst-support interactions on the CO_2 reduction activity of metalloporphyrins.

and PcM catalysts might also be affected by electronic coupling with CNTs,[68] fullerenes,[69,70] and other conductive supports.[71]

To better understand these effects, we employed discrete porphyrin nanocages (**M_2BiCage**, Scheme 1) to examine how molecular porosity and catalyst-support interactions affect the CO_2RR performance of metalloporphyrins. We recently reported the synthesis of unmetalled **H_4BiCage** and that this structure strongly binds the fullerenes C_{60} and C_{70} as guests.[72] Metalating **H_4BiCage** with Fe and Co provided CO_2RR catalysts that exhibit comparable porosity to many MOFs and COFs used for CO_2 reduction,[25–34,37] while association of C_{60}/C_{70} in the **M_2BiCages** provides a way to examine how the catalytic sites are affected by interactions with these carbon nanomaterials. Notably, the cages, their host-guest complexes, and related monomeric porphyrins (Scheme 1) all adsorb on carbon black to provide electrocatalytic inks with similarly high accessibilities of the metal sites to H^+ and e^-. By normalizing these mass/charge transport variables for the different catalysts, the local effects of the hollow cage structure and its interactions with fullerenes were elucidated. The host-guest complexes generally showed similar or better performance than the empty **M_2BiCages** for reducing CO_2 to CO, and in the case of **C_{70}@$(FeCl)_2$BiCage**, this behavior was leveraged to achieve some of the highest current densities for selective CO formation that have been observed using molecular catalysts operating at overpotentials milder than ≈0.5 V.[17,27,32,37,45,49,53,65]

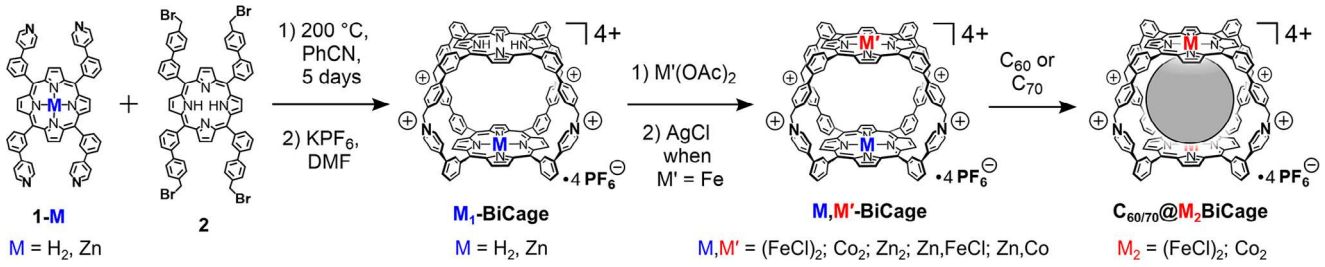

Scheme 2. Synthesis of metalloporphyrin nanocages **Zn_1BiCage**, **Zn,M-BiCage**, and **M_2BiCage** (M = Fe, Co), and the uptake of C_{60} and C_{70} by the **M_2BiCages**.

Results and Discussion

Synthesis and Characterization of the M_2BiCages

The two porphyrin faces of **H_4BiCage** are held together by four covalent pyridinium linkages,[72,73] providing a robust structure that was readily metallated[74] to provide **M_2BiCage**s (M = FeCl, Co) as catalysts for studying CO_2RR (Scheme 2). Iron and cobalt were chosen because PorCo and PcCo-based MOFs and COFs have been widely studied as CO_2RR catalysts,[25,27,29–40,44] and PorFe complexes were used in two of the only other discrete nanocages that have been examined for CO_2RR.[25,26] **Zn_2BiCage** was also prepared for comparison with the catalytically active **M_2BiCages**. Notably, by metalating one of the precursor porphyrins with Zn before assembling the cage, a monometallic **Zn_1BiCage** was prepared and subsequently metallated with Fe and Co to provide heterobimetallic **Zn,M-BiCages**. Metallation of the cages was confirmed by NMR and UV–vis spectroscopies (Figures S1–S17, S36–S48) as well as ESI-HRMS (Figures S21–S32). Likewise, NMR and ESI-HRMS characterization was used to confirm that the **M_2BiCages** quantitatively uptake C_{60} or C_{70} upon sonicating a suspension of these fullerenes in CD_3CN solutions of the hosts (Figures S2, S8–S10, S16, S22, S23, S30, S31).

Despite crystals of the **M_2BiCages** diffracting weakly, the structure of **Zn_2BiCage** was successfully determined by single-crystal XRD analysis, revealing that the benzylpyridinium linkers are arranged to provide a barrel-like pore with a hexagonal profile (Figure 1). Water molecules are bound to the zinc sites inside the cage, indicating the cage structure does not interfere with the coordination chemistry of the internal faces of the zinc porphyrins.

Interestingly, an inversion center is located between the two zinc sites despite the two halves of the cage being electronically distinct. Apparently, the benzylpyridinium linkers have a charge distribution that is even enough to allow the cage to pack in a way that reflects the geometric symmetry of its components rather than their electronic differences. Likewise, PF_6^- anions inside and outside the cage are placed symmetrically with respect to the distinct halves of the cage.

The **Zn_2BiCage** units are aligned to form 1D channels of ≈1 nm width (Figure 1c), which are packeted together in a distorted honeycomb-like motif (Figure 1d). This packing provides an extended porous structure reminiscent of many

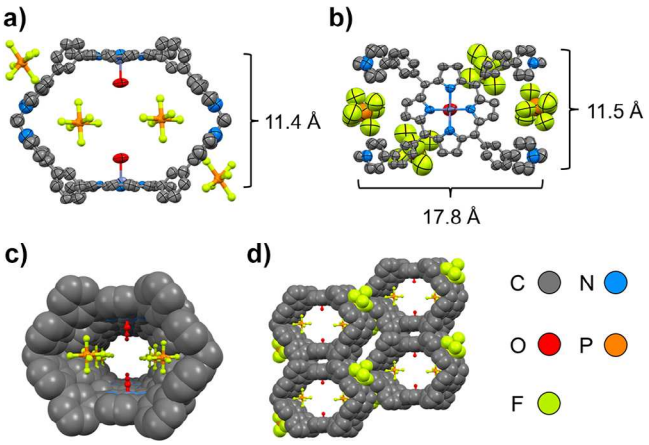

Figure 1. Structure of **$Zn(OH_2)_2$BiCage**•$4PF_6$ determined by single-crystal X-ray diffraction analysis (P-1, R_1 = 15.12%). a) View facing the hexagonal aperture of the cage. b) View facing a zinc-porphyrin wall. c) Infinite channel formed by the alignment of the **Zn_2BiCage** units. d) Honeycomb-like packing of the **Zn_2BiCage** units. Note that a mix of thermal ellipsoid, ball-and-stick, and space-filling representations are used in A – D, with ellipsoids set to 50% probability. Disordered solvent was excluded from the structure model.

MOFs and COFs that have been employed as CO_2RR catalysts.[26–34,37] Indeed, CO_2 sorption studies at 195 K (Figure S113) reveal that the **M_2BiCages** have BET surface areas (145 $m^2\ g^{-1}$, M = Zn; 155 $m^2\ g^{-1}$, M = Co; 293 $cm^2\ g^{-1}$, M = FeCl; Table S7) comparable to or a little lower than those of many MOFs,[28] COFs,[31,32,35–37,39,40] and nanocages[41] that have been used for CO_2RR.

Electrochemical Characterization of M_2BiCages

Initial electrochemical characterization of the **M_2BiCages** was performed by cyclic voltammetry in DMF solution (0.1 M $TBAPF_6$ electrolyte). Under these conditions, the metallated cages exhibit poorly reversible reductions of the pyridinium groups near −1.6 V (vs $Fc^{+/0}$), as well as reversible or quasi reversible redox couples that are characteristic of Fe, Co, and Zn porphyrins (Table 1 and Figure 2; Figure S1, S55, S56, S62).[75–77] These latter redox features overlap for the distinct porphyrin units of each cage, suggesting that both porphyrin faces have similar electronics. Additionally, the

Table 1: Potentials for the metal-centered and pyridinium-centered reductions of the **M_2BiCages** and related monomeric metalloporphyrins in DMF.[a]

PorM	M^{III}/M^{II}	M^{II}/M^{I}	*N*-alkyl-$py^{+/\bullet}$	$M^{I/0}$
$(FeCl)_2$BiCage[b]	−0.60	−1.54[c]	−1.54[c]	−2.14
xMePyPFeCl[b]	−0.62	−1.58[c]	−1.58[c]	−2.18
TPPFe[d]	−0.65	−1.53	N/A	−2.16
Co_2BiCage[b]	not observed[e]	−1.26	−1.61	−2.41
xMePyPCo[b]	not observed[e]	−1.19	−1.64	−2.43
TPPCo[f]	not observed[e]	−1.30	N/A	−2.43

[a] Potentials are $E_{1/2}$ values in V versus $Fc^{+/0}$ and rounded to the nearest 10 mV for (quasi)reversible redox couples. [b] This work. [c] The Fe^{II}/Fe^{I} and *N*-alkyl-$py^{+/\bullet}$ redox couples overlap. [d] Ref. [75]. [e] The Co^{III}/Co^{II} redox couple was not observed due to slow electron transfer kinetics. [f] Ref. [76].

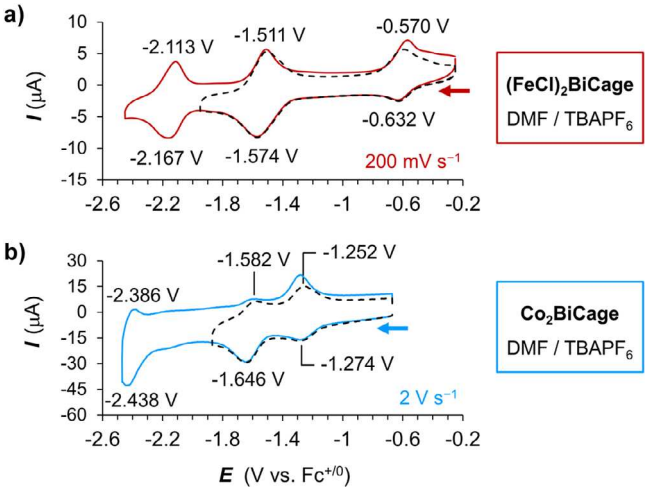

Figure 2. Cyclic voltammograms of 0.05 mM solutions of a) **$(FeCl)_2$BiCage**, and b) **Co_2BiCage** were recorded in DMF (0.1 M $TBAPF_6$ supporting electrolyte).

metal- and porphyrin-centered reductions occur at potentials similar to those of related neutral tetraphenylporphyrin complexes (Table 1; Figure S1),[75–77] indicating that the cationic cage does not strongly perturb the electronics of the metalloporphyrins.

The most negative reductions of the **$(FeCl)_2$-** and **Co_2-BiCages** show enhancements of current under 1 atm CO_2 (Figures S50, S58) consistent with the typical CO_2RR activity of iron- and cobalt- porphyrin complexes in organic solvents.[14,75] However, the stabilities and solubilities of the **M_2BiCages** are diminished under such strongly reducing conditions, as evident from the irreversible pyridinium reductions and other irregularities seen in CV measurements (Figures S49, S55–S57, S62). Given this limitation, as well as the unremarkable catalytic performance in preliminary screenings (i.e., high overpotentials typical of simpler porphyrin catalysts[14,75]), we did not further examine the CO_2RR activity of the **M_2BiCages** in DMF.

We next examined the electrochemistry of the **$(FeCl)_2$-** and **Co_2-BiCages** in aqueous electrolyte, which offers advantages for studying the CO_2RR activity of these structures. In particular, iron and cobalt porphyrins exhibit CO_2 reduction at milder potentials in water,[25–28,41–44] while more polar conditions should stabilize the cages against detrimental reductions of their cationic pyridinium groups, thus enabling CO_2RR activity at potentials in which the cages are reasonably stable. The **M_2BiCages** are not soluble in water even when paired with hydrophilic anions (e.g., SO_4^{2-}, HSO_4^-), so their aqueous electrochemistry was examined under heterogeneous conditions. The cages adsorb quantitatively onto carbon black from acetonitrile solution, leading to stable suspensions (Figure S63) that were used to deposit 25 nmol loadings of the cages (50 nmol M) onto 1 cm^2 carbon cloth electrodes. Notably, this simple electrode preparation led to nearly ideal surface-adsorbed CV responses for the **M_2BiCages** (Figure 3a,c), with a high percentage (40–70% range, typically ≈50%) of the metal sites accessible based on integrating the CVs of the electrodes (Table S3).

Cyclic voltammograms of **$(FeCl)_2$BiCage** under argon at pH 11 display Fe^{III}/Fe^{II} and Fe^{II}/Fe^{I} redox couples ($E_{1/2}$ = +0.434 and −0.223 V vs RHE) that are reversible at scan rates up to 100 mV s^{-1} before showing E_{pc}/E_{pa} separations suggesting rate-limiting electron transfer (Figure 3a).[78,79] The Fe^{III}/Fe^{II} redox couple maintains similar reversibility at lower pH, with a potential that shows a 52 mV per decade dependence on H^+ concentration (Figure S64), consistent with a $1H^+/1e^-$ reduction of $Fe^{III}OH$ to $Fe^{II}OH_2$.[80] The good reversibility of this reduction indicates that protons and electrons can readily access the iron sites of the cage, representing a useful feature since H^+ and e^- transport often limit electrocatalysis in other porous molecular materials.[19] Thus, the CO_2RR activity of **$(FeCl)_2$BiCages** should be biased toward revealing the beneficial effects of the porous cage structure. The **Co_2BiCage** displays only a weak and inconsistent Co^{III}/Co^{II} redox couple ($E_{1/2}$ = +0.759 V vs RHE at pH 7.2) that was not useful for evaluating H^+/e^- behavior, but its Co^{II}/Co^{I} reduction ($E_{1/2}$ = −0.172 V, Figure 3c) exhibits similar behavior to the Fe^{II}/Fe^{I} reduction of **$(FeCl)_2$BiCage**. Thus, the immobilized Co and Fe cages appear to have similar electron-transfer kinetics.

Aqueous Electrocatalytic Activity of the M_2BiCages

The Fe^{II}/Fe^{I} couple is invariant to pH and becomes partially obscured by the onset of H_2 evolution at pH 7.2 under argon (≈−0.44 V vs RHE, Figure 3b). The onset of catalysis and the Fe^{II}/Fe^{I} reduction are both shifted positively by >150 mV under 1 atm of CO_2 in the $KHCO_3$ electrolyte, indicating significant CO_2RR activity (Figure 3b). Similar CO_2RR activity is observed for **Co_2BiCage** (Figure 3d), though in this case, the M^{II}/M^{I} reduction maintains a constant potential that is positive of the onset of catalysis under both Ar and CO_2. Additionally, the onsets of CO_2RR and HER activity occur closer together (<100 mV) for **Co_2BiCage**, potentially indicating greater competition between CO_2 reduction and HER for this catalyst.

Applied potential electrolysis was used to further probe the CO_2RR activity of the **M_2BiCages** as well as several other catalysts that were examined for comparisons. Two

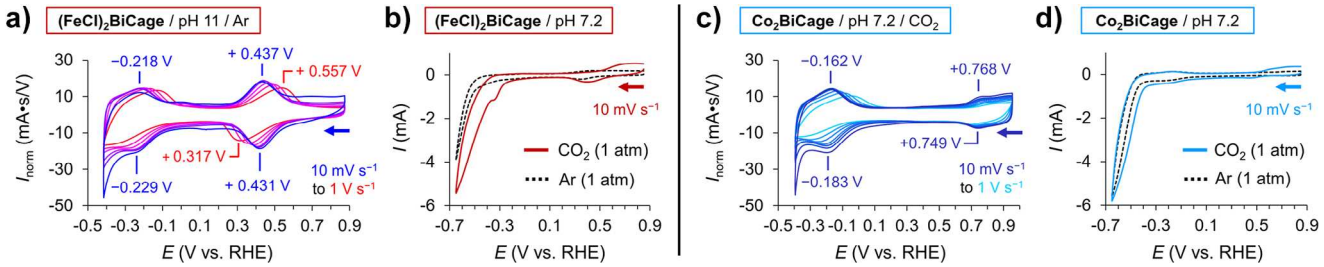

Figure 3. Aqueous CVs of **M_2BiCage**•$4PF_6$ adsorbed on carbon black (1:5 by weight) and drop cast on 1 cm^2 carbon cloth electrodes at 50 nmol metal loadings. a) **$(FeCl)_2$BiCage** at pH 11 and scan rates of 0.01, 0.05, 0.1, 0.25, 0.5 and 1 V s^{-1}. b) **$(FeCl)_2$BiCage** at pH 7.2 under Ar vs. CO_2. c) **Co_2BiCage** at pH 7.2 and scan rates of 0.01–1 V s^{-1}. d) **Co_2BiCage** at pH 7.2 under Ar vs. CO_2. Phosphate and carbonate buffers were used respectively for experiments under Ar vs. CO_2.

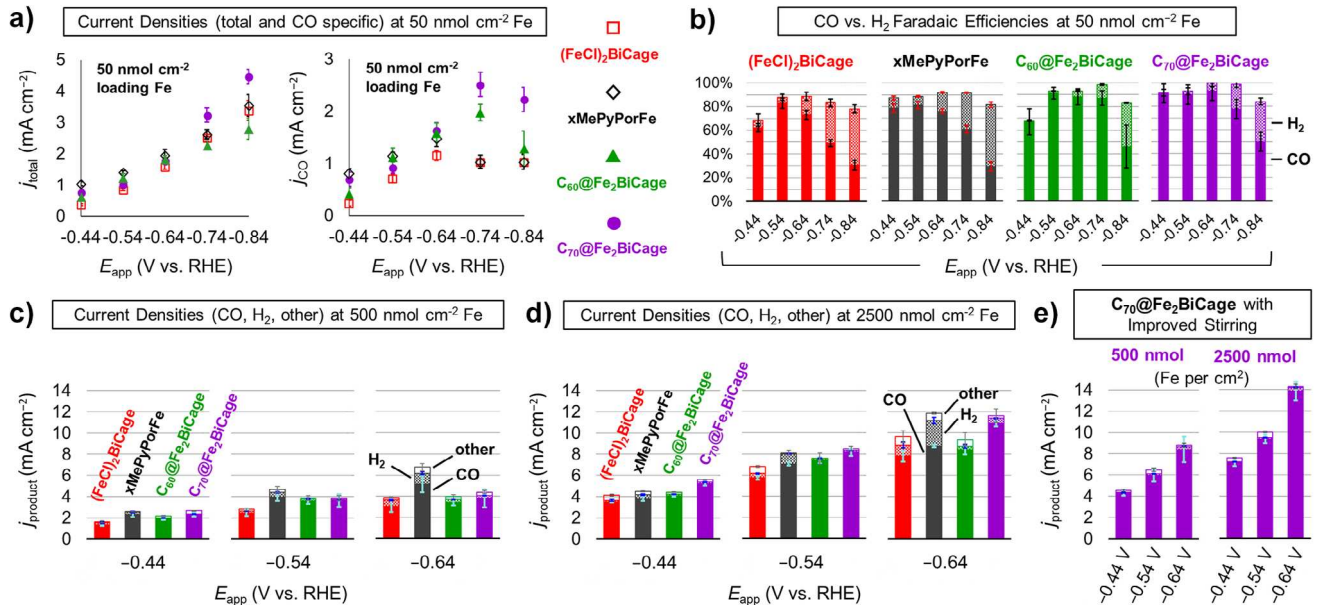

Figure 4. Heterogeneous CO_2RR activity of **$(FeCl)_2$BiCage**, **xMePyPFeCl**, and **C_{60}/C_{70}@$(FeCl)_2$BiCage** on 1 cm^2 electrodes (1 atm CO_2, 0.5 M $KHCO_3$). a) Average current densities and CO partial current densities over 1 h using 50 nmol loadings of Fe, and b) the corresponding CO and H_2 Faradaic efficiencies. c) Average current densities for formation of CO, H_2, and unidentified products over 1 h using 500 nmol loadings of Fe, d) using 2500 nmol loadings of Fe, and e) using 250 and 1250 nmol loadings of **C_{70}@$(FeCl)_2$BiCage** with the flow velocity across the electrode increased to ≈17 cm s^{-1} (≈1 cm s^{-1} was used in A – D).

tetracationic porphyrin complexes (**xMePyPM** and **xPyBzM**, Scheme 1) were examined as models for the two individual halves of the cages, and the host-guest complexes **C_{60}/C_{70}@M_2BiCages** were used to probe whether the internal pores of the cages or their interactions with fullerenes are better at promoting CO_2RR. Several other catalysts (TPPM, **Zn_2BiCage**, the **M,Zn-BiCages**) were also examined, but along with **xPyBzPM**, showed lower activity and/or selectivity than the **M_2BiCages**. Thus, only results from the **M_2BiCages**, their fullerene complexes, and the best monomeric catalysts (**xMePyPM**) are presented here (Figures 4 and 5). It is, however, worth noting that **(FeCl),Zn-BiCage** showed similar CO_2RR activity per iron site as **$(FeCl)_2$BiCage**, suggesting that both iron sites in **$(FeCl)_2$BiCage** have similar activity (see Figures S82–S84 for comparisons of all catalysts).

Initial experiments examined 50 nmol metal loadings of the iron catalysts deposited on 1 cm^2 electrodes using an optimized 1:5 mass ratio of cage to carbon black that was determined in preliminary screenings (Figure S81). The current response of each catalyst was then examined over 1 h at potentials from −0.34 to −0.94 V versus RHE in a cell with a frit-separated counter electrode. Faradaic efficiencies for gaseous products were determined by GC headspace analysis, revealing moderate to good activity and selectivity for CO formation in the range of −0.44 to −0.84 V (Figure 4a,b). Current densities increased similarly for the four best Fe catalysts from −0.44 to −0.64 V, with greater variation seen at −0.74 and −0.84 V (Figure 4a). Interestingly, at these latter potentials, the host-guest complexes **C_{70}@$(FeCl)_2$BiCage** and **C_{60}@$(FeCl)_2$BiCage** respectively give the highest and lowest total current densities, but the C_{60} complex ends up second to the C_{70} complex with respect to CO specific current densities. Thus, the fullerenes alter both the activity and selectivity of the porphyrin catalysts. Indeed, **$(FeCl)_2$BiCage** and **xMePyPFeCl** have maximum selectivities of ≈80% for CO formation at −0.54 V, while the host-guest complexes

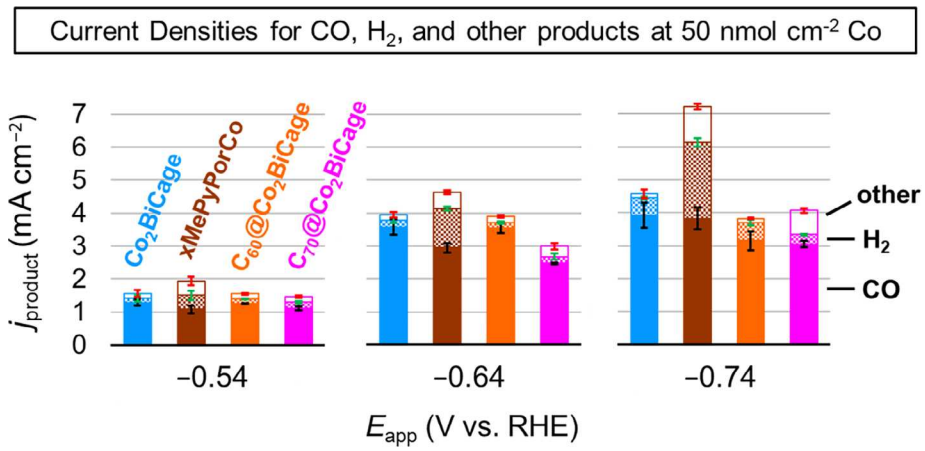

Figure 5. Heterogeneous CO_2RR activity of **Co_2BiCage**, **xMePyPCo**, and **C_{60}/C_{70}@CoBiCage** at 50 nmol loadings of Co on 1 cm^2 electrodes with an electrolyte (0.5 M $KHCO_3$, 1 atm CO_2) flow velocity of ≈1 cm s^{-1}. Average current densities are presented for the formation of CO, H_2, and unidentified other products.

both reach ≈90% CO selectivities at this voltage (Figure 4b). The host-guest complexes also maintain their selectivity better at negative potentials (Figure 4b), whereas the CO_2RR activity of **$(FeCl)_2$BiCage** and **xMePyPFeCl** gives way to significant H_2 formation at potentials ≤−0.64 V.

Good electrochemical accessibility (≥ 50%) was maintained for the four catalysts at increased metal loadings of 500 and 2500 nmol cm^{-2} (Figure S108, Table S3), so their activities were examined at these loadings, focusing on potentials (−0.44 to −0.64 V vs RHE) that yielded CO selectivities of ≥90% for some of the catalysts at lower loadings. Increased total current densities were obtained at higher loadings of all four catalysts (Figure 4c,d), with average increases of about 3-fold seen between 50 and 500 nmol cm^{-2}, and 2-fold between 500 and 2500 nmol cm^{-2}. Selectivity for CO formation was also improved for **$(FeCl)_2$BiCage** and its host-guest complexes, leading **C_{70}@$(FeCl)_2$BiCage** in particular to display excellent CO Faradaic efficiencies of ∼95% from −0.44 to −0.64 V versus RHE at the highest loading (Figure 4d; Figure S89). Other patterns of activity were similar to those at lower loadings. Thus, **$(FeCl)_2$BiCage** was the least active catalyst for CO production at most loadings and potentials; **xMePyPFeCl** showed good activity but the lowest selectivity for CO formation; and the host-guest complexes consistently had both good activity and selectivity for CO production, with **C_{70}@$(FeCl)_2$BiCage** consistently showing better performance than the other catalysts at 2500 nmol cm^{-2} loadings of Fe (Figure 4d).

Many immobilized molecular electrocatalysts only show good activity per metal site at low overall loadings.[21,26,41] For example, maximum electrochemically accessible iron loadings of just 3.7 nmol cm^{-2} were reported for the only other iron-porphyrin nanocage that has been examined for CO_2 reduction, limiting $|j_{CO}|$ to ≤1.6 mA cm^{-2} even at high overpotentials (−0.83 V vs RHE at pH 7.2, η = 0.71 V).[41] Thus, it is notable that **$(FeCl)_2$BiCage** and its host-guest complexes show improvements in activity with increased loadings even up to 2500 nmol cm^{-2} of Fe. The performance of **C_{70}@$(FeCl)_2$BiCage** was further improved simply by stirring the electrolyte more vigorously to increase its velocity across the electrode surface from ≈1 to ≈17 cm s^{-1}. This led to average increases in CO-specific current densities of about 90% when using Fe loadings of 500 nmol cm^{-2} at potentials from −0.44 to −0.64 V versus RHE, with selectivity for CO formation remaining above 90% (Figure 4e). Smaller increases in j_{CO} (≤ 37%) were attained upon further increasing iron loadings to 2500 nmol cm^{-2}. Nevertheless, the current densities for CO formation at this higher loading (j_{CO} = −7.2 mA cm^{-2} at −0.44 V, −9.4 mA cm^{-2} at −0.54 V, −13.9 mA cm^{-2} at −0.64 V vs RHE; all with FE_{CO} ≥94%) are among the best achieved for heterogenized molecular catalysts at these moderate potentials in simple frit-separated cells (Figure S91).[17,27,32,35,37–39,48,50,53,62,65,66,69] The CO-specific current density of −7.2 mA cm^{-2} at −0.44 V versus RHE (η = 320 mV) is especially notable, exceeding that achieved with all but a few molecular catalysts at such a mild potential.[17,50,53] Unfortunately, activity was diminished upon repeated catalytic runs (Figures S105, S106), leading current densities to be decreased by at least 20% after 6 h using 500 or 2500 nmol cm^{-2} loadings of iron.

We next examined the aqueous CO_2 reduction activity of **Co_2BiCage** and the other cobalt catalysts at Co loadings of 50 nmol cm^{-2}. Empty **Co_2BiCage** showed the best performance, giving CO selectivities of 80–90% at potentials of −0.54, −0.64, and −0.74 V versus RHE, with CO specific current densities of ≈−1.3, −3.5, and −3.9 mA cm^{-2} attained at these voltages (Figure 5). In comparison, the monomeric catalyst **xMePyPCo** showed worse activity and much lower selectivity for CO formation, while the host-guest complexes **C_{60}/C_{70}@Co_2BiCage** showed activities and selectivities for CO formation that were similar or slightly worse than those of the empty cage. Thus, the activity of **Co_2BiCage** is not improved by interactions with fullerenes.

Nevertheless, **Co_2BiCage** is a good catalyst by itself, requiring just 50 nmol cm^{-2} of Co to achieve current densities comparable to or exceeding those of most MOF and COF-based catalysts at higher loadings (≈500 nmol cm^{-2}).[31,32,44,65,69] As a result, **Co_2BiCage** has a turnover frequency (1333 h^{-1} measured against all Co sites) at a moderate overpotential (E_{app} = −0.64 V vs RHE, η =

520 mV) that is among the highest achieved by a molecularly defined porous material under similar experimental conditions (Figure S92A).[28,34,41,62] It is, however, worth noting that other catalyst-support materials (e.g., CNTs) can lead to much higher TOFs (Figure S92B).[17,50,53]

Increased loadings of **Co_2BiCage** led to improvements of CO_2RR performance that were relatively sensitive to the specific experimental conditions. For example, with gentle stirring (≈1 cm s^{-1} flow velocity) at −0.64 V versus RHE, 500 and 2500 nmol cm^{-2} loadings of cobalt led to improved j_{CO} values of −5.0 and −9.5 mA cm^{-2}, respectively, but with diminished selectivity (FE_{CO} = 77% and 72%, Figures S87, S90). Vigorous stirring (≈17 cm s^{-1} flow velocity) improved both the selectivity and current density for CO formation using 500 nmol cm^{-2} loadings of Co at −0.64 V versus RHE ($j_{CO} = -10.2$ mA cm^{-2}, $FE_{CO} = 92\%$), and good performance was also attained at higher and lower potentials (j_{CO} = −5.5 mA cm^{-2}, FE_{CO} = 85%, −0.54 V; j_{CO} = −16.6 mA cm^{-2}, $FE_{CO} = 89\%$, −0.74 V, Figure S87). In contrast, cobalt loadings of 2500 nmol cm^{-2} led to increased H_2 formation without further increases in CO_2RR (Figure S90). Thus, the activity and selectivity of **Co_2BiCage** do not scale as well as for the iron catalysts. However, the catalytic stability of **Co_2BiCage** at high loadings is far superior, showing a <10% decrease in total current after 6 h and no decrease in CO specific current over this timeframe (Figure S107).

Effects of Porosity versus Host-Guest Chemistry on CO_2RR

We sought to understand how the **M_2BiCage** structures and their interactions with fullerenes affect catalysis. First, it was noted that better activity and selectivity for CO formation correlate with better preservation of the redox features of a given catalyst after catalysis. For example, the Fe^{III}/Fe^{II} couple is maintained better in CVs of **C_{60}/C_{70}@$(FeCl)_2$BiCage** than in CVs of **$(FeCl)_2$BiCage** or **xMePyPFeCl** after 1 h of electrolysis at potentials down to −0.74 V versus RHE, and none of the catalysts are stable under more reducing conditions that give rise mainly to HER (Figures S93–S96). There is also a correlation between decreases in the redox features of the catalysts and decreases in CO_2 reduction activity upon repeated 1 h runs (Figure S106). These observations suggest that the active catalysts are the cages and other metalloporphyrin species as initially deposited on electrodes.

XPS spectra were similar for the catalysts as bulk powders or incorporated into inks, in all cases showing peaks with the expected binding energies for Fe, Co, and N in the context of pyridinium-substituted porphyrin complexes (Figures S114–S122).[81–83] Thus, the catalysts do not appear to be affected much by adsorption on carbon black, though small changes in the broadness of the pyridinium N-atom peaks (binding energy ≈402 eV) suggest that the chemical environment of the pyridiniums may be altered slightly. These peaks were broadened more after catalysis (Figures S115–S122), possibly indicating degradation of the pyridiniums or simply further alteration of their surrounding environment, e.g., by replacement of the PF_6^- anions.

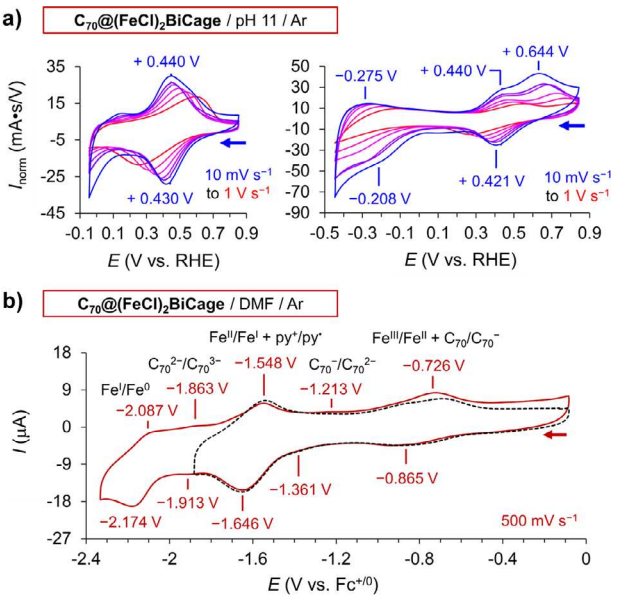

Figure 6. a) Variable scan rate CVs in aqueous conditions at different potential windows for **C_{70}@$(FeCl)_2$BiCage**•$4PF_6$ deposited on a 1 cm^{-2} carbon cloth electrode (50 nmol metal loading). b) CV of a 0.1 mM solution of the host-guest complex **C_{70}@$(FeCl)_2$BiCage** in DMF containing 0.1 M $TBAPF_6$.

The **M_2BiCages** were estimated to stack 1–4 layers deep when adsorbed on carbon black based on electrochemical surface areas measured capacitively for these inks (Figure S80).[84] Thus, the high accessibility of the metal sites (≈50%) likely comes from good dispersal of the cages on carbon rather than from their well-defined pores, especially since **xMePyPFeCl** also shows high accessibility (Table S3). Furthermore, SEM images show that cage-functionalized carbon black deposits more evenly on carbon cloth than does unfunctionalized carbon black (Figure S123), indicating that the high electrochemical accessibility of the immobilized **M_2BiCages** is due to features of their inks that arise at a scale beyond that of the molecular cage structure.

The cavity in the **M_2BiCages** might still benefit CO_2RR via the favorable uptake of CO_2, as is often suggested in the study of electrocatalytic materials with well-defined pores.[26,27,29,31–36,41,43,44,55,56] However, **C_{70}@$(FeCl)_2$BiCage** consistently shows better activity and selectivity for CO formation than attained with the empty bis-iron cage, and **C_{60}@Co_2BiCage** displays similar CO_2 reduction performance to **Co_2BiCage**. Since the fullerene guests take up nearly all the space between the porphyrin walls of the cage, especially for complexes of C_{70},[72,85] these observations indicate that good catalytic performance can be achieved even when the cavity of the **M_2BiCages** is blocked. This conclusion does not rule out the possibility that the internal pore aids CO_2 reduction in the empty **M_2BiCages**, but it does show that other effects can lead to similar or greater increases in activity and selectivity.

We next turned to understand how fullerenes enhance the CO_2RR activity of the **$(FeCl)_2$BiCage**. Cyclic voltammograms of **C_{60}/C_{70}@$(FeCl)_2$BiCage** inks at pH 11 (Figure 6a; Figures S65, S66) reveal that the Fe^{III}/Fe^{II} redox couples are similar to that of empty **$(FeCl)_2$BiCage** (Figure 3a), but the Fe^{II}/Fe^{I}

reductions of the host-guest complexes are larger, broader, and less reversible. The increased current suggests that the reduction of the fullerenes coincides with the Fe^{II}/Fe^{I} reduction, while the flattening of this wave at higher scan rates indicates slower electron transfer kinetics than for the empty bis-iron cage. Thus, while C_{60} has been used to aid electron transport in porous materials,[70,86,87] fullerene guests appear to slow the Fe^{II}/Fe^{I} kinetics of **$(FeCl)_2$BiCage**. This effect also appears to apply to the cobalt derivatives, since a Co^{II}/Co^{I} redox couple is not observed clearly for inks of **C_{60}/C_{70}@Co_2BiCage** (Figures S74, S76).

Electronic coupling between iron sites and fullerenes is another factor that might benefit CO_2RR activity.[69–71] Homogeneous CVs of **C_{60}/C_{70}@$(FeCl)_2$BiCage** in DMF (Figure 6; Figures S51, S52, and Table S2) reveal that the Fe^{III}/Fe^{II} reduction is shifted negatively by a moderate amount ($\Delta E_{1/2} \approx -0.2$ V vs $Fc^{+/0}$) relative to that of the empty cage (Table 1), while the Fe^{II}/Fe^{I} redox couple is not altered much by the fullerenes ($\Delta E_{1/2} \approx -0.05$ V). These results show that the redox features of the iron centers can be influenced by the fullerenes,[88–90] but suggest against strong metal-fullerene electronic interactions in the reduced states of the cage relevant to catalysis. Thus, metal-fullerene interactions might have some influence on catalytic activity, but it seems unlikely that electronic effects are primarily responsible for improving the CO_2RR performance of the host-guest complexes, especially since C_{60} and C_{70} both similarly affect the redox behavior of **$(FeCl)_2$BiCage** but C_{70} consistently leads to greater improvements in activity. Additionally, the fullerene guests appear to undergo significant chemical changes during catalysis, as evident from ESI-HRMS analysis of the host-guest complexes extracted from electrodes using DMSO after 3 h of continuous use catalyzing CO_2RR. The mass spectra are dominated by peaks consistent with substantial oxygenation and hydroxylation[91] of the fullerenes still bound in **Fe_2BiCage** (Figures S34, S35). Thus, the initial electronic properties of the fullerene guests are unlikely to be retained during electrolysis.

With electronic factors largely ruled out, structural effects appear to be the most consistent explanation for the influence of fullerenes on the activity of the **M_2BiCages**. Fullerene guests should alter the geometry and rigidity of the cages,[92–94] which would plausibly influence the activity and stability of these catalysts. This mechanistic interpretation would explain why C_{70} has a greater influence on catalytic activity than C_{60}, since the larger guest should alter the geometry and rigidity of the cages to a greater extent. However, we caution that it is difficult to confirm these possibilities experimentally, and reliable computational studies of these large host-guest systems are impractical within the scope of the present study.

Conclusion

The covalently linked **BiCage** motif was used to prepare several bimetallic bis-porphyrin nanocages, including heterobimetallic examples. The solution processibility of the **M_2BiCages** enabled facile hybridization of these structures with carbon black to provide electrocatalytic inks in which ≈50% of the metal sites are accessible to H^+ and e^-. This high electrochemical addressability is superior to that of most other molecularly defined porous materials that have been examined as electrocatalysts for CO_2RR,[26,29,31,37] allowing the metallated cages and their complexes with C_{60} and C_{70} to achieve good activity for reducing CO_2 to CO. Notably, the performance of the **M_2BiCages** and their fullerene complexes **C_{60}/C_{70}@M_2BiCage** at low overpotentials exceeds that of the few other nanocages that have been examined as catalysts for this reaction.[41–44] Moreover, by some metrics, the **M_2BiCages** and their host-guest complexes are among the best nanoporous electrocatalysts in general for CO formation at low overpotentials.[17,28,34,41,50,62]

Nevertheless, like other porous catalysts, the **M_2BiCages** would require significant improvements to achieve CO_2RR performance that is of practical use. Thus, our most salient findings are the mechanistic insights afforded by studying these well-defined porous catalysts. In particular, **$(FeCl)_2$BiCage** and **Co_2BiCage** both exhibit better selectivity and, in some cases, better activity for CO formation than their monomeric counterparts **xMePyPM**. Such findings are often attributed to beneficial effects of porosity in materials such as MOFs,[25,27] COFs,[29,31–36] and other nanocages.[41,43,44,55,56] However, comparisons of the **M_2BiCages** and their fullerene complexes reveal that the internal cavity of the cages is not needed for good CO_2RR activity. Thus, more caution may be warranted when interpreting how nanoporous support materials affect the activity of immobilized CO_2RR catalysts. We propose that pore-blocking experiments could be developed more widely for testing whether confined metal sites actually contribute to the electrocatalytic activity of these materials.

In another notable finding, the association of C_{70} in **$(FeCl)_2$BiCage** leads to improved catalytic performance. Neither enhanced electron transfer kinetics nor metal-fullerene electronic interactions appear to underly this behavior, suggesting that the C_{70} guest boosts CO_2RR in a different manner than usually invoked for fullerenes and, especially, their extended CNT counterparts.[45–54,68–70] Though the C_{70} guest improves the activity of **C_{70}@$(FeCl)_2$BiCage**, this catalyst does not achieve TOFs nearly as high as those often reported for molecular catalysts adsorbed on carbon nanotubes.[17,50,53] Thus, despite the excellent electrochemical accessibility of our nanocages when immobilized, their local interactions with fullerenes are not able to match the benefits conferred by securing molecular electrocatalysts to more conductive CNT supports.

Supporting Information

The authors have cited additional references within the Supporting Information.[95–108]

Acknowledgements

M.C.L acknowledges the ACS Petroleum Research Fund (PRF grant #61015-DNI3) and the National Science Foun-

dation (CHE award #2204045 and #2117792) for financial support of this research. The National Science Foundation is also acknowledged for grant CHE-2117792 for the acquisition of the X-ray diffractometer used in this study. Lastly, the authors acknowledge Dr. Peter Smith for helpful discussions of electrochemical ink preparation, Dr. Demyan Prokopchuk and Lirong Lin for assistance with the collection of ^{13}C NMR data, Dr. Kate M. Waldie and Dr. G. Charles Dismukes for the use of their potentiostats, and Iram F. Mansoor for experimental assistance.

Conflict of Interests

The authors declare no conflict of interest.

Data Availability Statement

The data that support the findings of this study are available in the supplementary material of this article and via the Cambridge Crystallographic Data Centre and the Fachinformationszentrum Karlsruhe Access Structure service.[109]

Keywords: C1 Building Blocks · Catalysis · Electrochemistry · Porphyrinoids · Supramolecular chemistry

[1] E. E. Benson, C. P. Kubiak, A. J. Sathrum, J. M. Smieja, *Chem. Soc. Rev.* **2009**, *38*, 89–99.
[2] P. De Luna, C. Hahn, D. Higgins, S. A. Jaffer, T. F. Jaramillo, E. H. Sargent, *Science* **2019**, *364*, eaav3506.
[3] R. I. Masel, Z. Liu, H. Yang, J. J. Kaczur, D. Carrillo, S. Ren, D. Salvatore, C. P. Berlinguette, *Nat. Nanotechnol.* **2021**, *16*, 118–128.
[4] F.-Y. Gao, R.-C. Bao, M.-R. Gao, S.-H. Yu, *J. Mater. Chem. A* **2020**, *8*, 15458–15478.
[5] S. Lamaison, D. Wakerley, J. Blanchard, D. Montero, G. Rousse, D. Mercier, P. Marcus, D. Taverna, D. Giaume, V. Mougel, M. Fontecave, *Joule* **2020**, *4*, 395–406.
[6] M. C. O. Monteiro, M. F. Philips, K. J. P. Schouten, M. T. M. Koper, *Nat. Commun.* **2021**, *12*, 4943.
[7] C. Costentin, J.-M. Savéant, *Nat. Rev. Chem.* **2017**, *1*, 0087.
[8] A. M. Appel, M. L. Helm, *ACS Catal.* **2014**, *4*, 630–633.
[9] C. Costentin, M. Robert, J.-M. Savéant, A. Tatin, *Proc. Natl. Acad. Sci. USA* **2015**, *112*, 6882–6886.
[10] P. Gotico, B. Boitrel, R. Guillot, M. Sircoglou, A. Quaranta, Z. Halime, W. Leibl, A. Aukauloo, *Angew. Chem. Int. Ed.* **2019**, *58*, 4504–4509.
[11] M. R. Narouz, P. De La Torre, L. An, C. J. Chang, *Angew. Chem. Int. Ed.* **2022**, *61*, e202207666.
[12] Branch, J. J. W., *ACS Catal.* **2023**, *13*, 3902–3912.
[13] K. Teindl, B. O. Patrick, E. M. Nichols, *J. Am. Chem. Soc.* **2023**, *145*, 17176–17186.
[14] D. Behar, T. Dhanasekaran, P. Neta, C. M. Hosten, D. Ejeh, P. Hambright, E. Fujita, *J. Phys. Chem. A* **1998**, *102*, 2870–2877.
[15] S. Meshitsuka, M. Ichikawa, K. Tamaru, *J. Chem. Soc. Chem. Commun.* **1974**, 158.
[16] L. Yao, K. E. Rivera-Cruz, P. M. Zimmerman, N. Singh, C. C. L. McCrory, *ACS Catal.* **2024**, *14*, 366–372.
[17] M. Wang, K. Torbensen, D. Salvatore, S. Ren, D. Joulié, F. Dumoulin, D. Mendoza, B. Lassalle-Kaiser, U. Işci, C. P. Berlinguette, M. Robert, *Nat. Commun.* **2019**, *10*, 3602.
[18] C. Costentin, J.-M. Savéant, *Curr. Opin. Electrochem.* **2019**, *15*, 58–65.
[19] S. Banerjee, R. I. Anayah, C. S. Gerke, V. S. Thoi, *ACS Cent. Sci.* **2020**, *6*, 1671–1684.
[20] Y. Wu, Y. Liang, H. Wang, *Acc. Chem. Res.* **2021**, *54*, 3149–3159.
[21] M. Zhu, R. Ye, K. Jin, N. Lazouski, K. Manthiram, *ACS Energy Lett.* **2018**, *3*, 1381–1386.
[22] S. Ren, D. Joulié, D. Salvatore, K. Torbensen, M. Wang, M. Robert, C. P. Berlinguette, *Science* **2019**, *365*, 367–369.
[23] K. Torbensen, C. Han, B. Boudy, N. Von Wolff, C. Bertail, W. Braun, M. Robert, *Chem. - Eur. J.* **2020**, *26*, 3034–3038.
[24] S. Sinha, R. Zhang, J. J. Warren, *ACS Catal.* **2020**, *10*, 12284–12291.
[25] N. Kornienko, Y. Zhao, C. S. Kley, C. Zhu, D. Kim, S. Lin, C. J. Chang, O. M. Yaghi, P. Yang, *J. Am. Chem. Soc.* **2015**, *137*, 14129–14135.
[26] B.-X. Dong, S.-L. Qian, F.-Y. Bu, Y.-C. Wu, L.-G. Feng, Y.-L. Teng, W.-L. Liu, Z.-W. Li, *ACS Appl. Energy Mater.* **2018**, *1*, 4662–4669.
[27] R. Matheu, E. Gutierrez-Puebla, M. Á. Monge, C. S. Diercks, J. Kang, M. S. Prévot, X. Pei, N. Hanikel, B. Zhang, P. Yang, O. M. Yaghi, *J. Am. Chem. Soc.* **2019**, *141*, 17081–17085.
[28] H. Zhong, M. Ghorbani-Asl, K. H. Ly, J. Zhang, J. Ge, M. Wang, Z. Liao, D. Makarov, E. Zschech, E. Brunner, I. M. Weidinger, J. Zhang, A. V. Krasheninnikov, S. Kaskel, R. Dong, X. Feng, *Nat. Commun.* **2020**, *11*, 1409.
[29] S. Lin, C. S. Diercks, Y.-B. Zhang, N. Kornienko, E. M. Nichols, Y. Zhao, A. R. Paris, D. Kim, P. Yang, O. M. Yaghi, C. J. Chang, *Science* **2015**, *349*, 1208–1213.
[30] C. S. Diercks, S. Lin, N. Kornienko, E. A. Kapustin, E. M. Nichols, C. Zhu, Y. Zhao, C. J. Chang, O. M. Yaghi, *J. Am. Chem. Soc.* **2018**, *140*, 1116–1122.
[31] B. Han, X. Ding, B. Yu, H. Wu, W. Zhou, W. Liu, C. Wei, B. Chen, D. Qi, H. Wang, K. Wang, Y. Chen, B. Chen, J. Jiang, *J. Am. Chem. Soc.* **2021**, *143*, 7104–7113.
[32] B. Han, Y. Jin, B. Chen, W. Zhou, B. Yu, C. Wei, H. Wang, K. Wang, Y. Chen, B. Chen, J. Jiang, *Angew. Chem. Int. Ed.* **2022**, *61*, e202114244.
[33] L. Gong, B. Chen, Y. Gao, B. Yu, Y. Wang, B. Han, C. Lin, Y. Bian, D. Qi, J. Jiang, *Inorg. Chem. Front.* **2022**, *9*, 3217–3223.
[34] S.-Y. Chi, Q. Chen, S.-S. Zhao, D.-H. Si, Q.-J. Wu, Y.-B. Huang, R. Cao, *J. Mater. Chem. A* **2022**, *10*, 4653–4659.
[35] Q. Wu, D.-H. Si, Q. Wu, Y.-L. Dong, R. Cao, Y.-B. Huang, *Angew. Chem. Int. Ed.* **2023**, *62*, e202215687.
[36] X. Yang, X. Li, M. Liu, S. Yang, Q. Xu, G. Zeng, *Angew. Chem. Int. Ed.* **2024**, *63*, e202317785.
[37] Y. Yue, P. Cai, K. Xu, H. Li, H. Chen, H.-C. Zhou, N. Huang, *J. Am. Chem. Soc.* **2021**, *143*, 18052–18060.
[38] Y. Song, J.-J. Zhang, Z. Zhu, X. Chen, L. Huang, J. Su, Z. Xu, T. H. Ly, C.-S. Lee, B. I. Yakobson, B. Z. Tang, R. Ye, *Appl. Catal. B.* **2021**, *284*, 119750.
[39] Y. Zhang, X. Zhang, L. Jiao, Z. Meng, H.-L. Jiang, *J. Am. Chem. Soc.* **2023**, *145*, 24230–24239.
[40] M.-D. Zhang, D.-H. Si, J.-D. Yi, S.-S. Zhao, Y.-B. Huang, R. Cao, *Small* **2020**, *16*, 2005254.
[41] P. T. Smith, B. P. Benke, Z. Cao, Y. Kim, E. M. Nichols, K. Kim, C. J. Chang, *Angew. Chem. Int. Ed.* **2018**, *57*, 9684–9688.
[42] A. K. Surendran, G. L. Tripodi, E. Pluhařová, A. Y. Pereverzev, J. P. J. Bruekers, J. A. A. W. Elemans, E. J. Meijer, J. Roithová, *Nat. Sci.* **2023**, *3*, e20220019.
[43] Y. Hu, S. Huang, L. J. Wayment, J. Wu, Q. Xu, T. Chang, Y.-P. Chen, X. Li, B. Andi, H. Chen, Y. Jin, H. Zhu, M. Du, S. Lu, W. Zhang, *Cell Rep. Phys. Sci.* **2023**, *4*, 101285.

[44] X. Liu, C. Liu, X. Song, X. Ding, H. Wang, B. Yu, H. Liu, B. Han, X. Li, J. Jiang, *Chem. Sci.* **2023**, *14*, 9086–9094.
[45] I. Bhugun, D. Lexa, J.-M. Saveant, *J. Am. Chem. Soc.* **1994**, *116*, 5015–5016.
[46] A. Maurin, M. Robert, *Chem. Commun.* **2016**, *52*, 12084–12087.
[47] X. Zhang, Z. Wu, X. Zhang, L. Li, Y. Li, H. Xu, X. Li, X. Yu, Z. Zhang, Y. Liang, H. Wang, *Nat. Commun.* **2017**, *8*, 14675.
[48] X.-M. Hu, M. H. Rønne, S. U. Pedersen, T. Skrydstrup, K. Daasbjerg, *Angew. Chem. Int. Ed.* **2017**, *56*, 6468–6472.
[49] M. Zhu, J. Chen, L. Huang, R. Ye, J. Xu, Y.-F. Han, *Angew. Chem. Int. Ed.* **2019**, *58*, 6595–6599.
[50] M. Abdinejad, L. F. B. Wilm, F. Dielmann, H. B. Kraatz, *ACS Sustain. Chem. Eng.* **2021**, *9*, 521–530.
[51] X. Zhang, Y. Wang, M. Gu, M. Wang, Z. Zhang, W. Pan, Z. Jiang, H. Zheng, M. Lucero, H. Wang, G. E. Sterbinsky, Q. Ma, Y.-G. Wang, Z. Feng, J. Li, H. Dai, Y. Liang, *Nat. Energy* **2020**, *5*, 684–692.
[52] C. L. Rooney, M. Lyons, Y. Wu, G. Hu, M. Wang, C. Choi, Y. Gao, C.-W. Chang, G. W. Brudvig, Z. Feng, H. Wang, *Angew. Chem. Int. Ed.* **2024**, *63*, e202310623.
[53] M. Wang, L. Chen, T.-C. Lau, M. Robert, *Angew. Chem. Int. Ed.* **2018**, *57*, 7769–7773.
[54] A. Zhanaidarova, S. C. Jones, E. Despagnet-Ayoub, B. R. Pimentel, C. P. Kubiak, *J. Am. Chem. Soc.* **2019**, *141*, 17270–17277.
[55] P. De La Torre, L. An, C. J. Chang, *Adv. Mater.* **2023**, *35*, 2302122.
[56] S. Lu, H. Hu, H. Sun, F. Yang, H. Zhu, M. Du, Y. Jin, W. Zhang, *Green Chem.* **2024**, *26*, 5744–5769.
[57] R. Shimoni, Z. Shi, S. Binyamin, Y. Yang, I. Liberman, R. Ifraemov, S. Mukhopadhyay, L. Zhang, I. Hod, *Angew. Chem. Int. Ed.* **2022**, *61*, e202206085.
[58] Y. Guo, W. Shi, H. Yang, Q. He, Z. Zeng, J.-y. Ye, X. He, R. Huang, C. Wang, W. Lin, *J. Am. Chem. Soc.* **2019**, *141*, 17875–17883.
[59] K. Leung, I. M. B. Nielsen, N. Sai, C. Medforth, J. A. Shelnutt, *J. Phys. Chem. A* **2010**, *114*, 10174–10184.
[60] D. J. Martin, J. M. Mayer, *J. Am. Chem. Soc.* **2021**, *143*, 11423–11434.
[61] L. S. Xie, G. Skorupskii, M. Dincă, *Chem. Rev.* **2020**, *120*, 8536–8580.
[62] Y.-R. Wang, Q. Huang, C.-T. He, Y. Chen, J. Liu, F.-C. Shen, Y.-Q. Lan, *Nat. Commun.* **2018**, *9*, 4466.
[63] Q. Wu, R.-K. Xie, M.-J. Mao, G.-L. Chai, J.-D. Yi, S.-S. Zhao, Y.-B. Huang, R. Cao, *ACS Energy Lett.* **2020**, *5*, 1005–1012.
[64] H.-J. Zhu, M. Lu, Y.-R. Wang, S.-J. Yao, M. Zhang, Y.-H. Kan, J. Liu, Y. Chen, S.-L. Li, Y.-Q. Lan, *Nat. Commun.* **2020**, *11*, 497.
[65] N. Huang, K. H. Lee, Y. Yue, X. Xu, S. Irle, Q. Jiang, D. Jiang, *Angew. Chem. Int. Ed.* **2020**, *59*, 16587–16593.
[66] Z. Meng, J. Luo, W. Li, K. A. Mirica, *J. Am. Chem. Soc.* **2020**, *142*, 21656–21669.
[67] X. Zhang, Y.-Z. Yuan, H.-F. Li, Q.-J. Wu, H.-J. Zhu, Y.-L. Dong, Q. Wu, Y.-B. Huang, R. Cao, *Mater. Chem. Front.* **2023**, *7*, 2661–2670.
[68] J. Su, C. B. Musgrave, Y. Song, L. Huang, Y. Liu, G. Li, Y. Xin, P. Xiong, M. M.-J. Li, H. Wu, M. Zhu, H. M. Chen, J. Zhang, H. Shen, B. Z. Tang, M. Robert, W. A. Goddard, R. Ye, *Nat. Catal.* **2023**, *6*, 818–828.
[69] Z. Xin, Y.-R. Wang, Y. Chen, W.-L. Li, L.-Z. Dong, Y.-Q. Lan, *Nano Energy* **2020**, *67*, 104233.
[70] X. Dong, Z. Xin, D. He, J.-L. Zhang, Y.-Q. Lan, Q.-F. Zhang, Y. Chen, *Chin. Chem. Lett.* **2023**, *34*, 107459.
[71] M. Abdinejad, A. Farzi, R. Möller-Gulland, F. Mulder, C. Liu, J. Shao, J. Biemolt, M. Robert, A. Seifitokaldani, T. Burdyny, *Nat. Catal.* **2024**, *7*, 1109–1119.
[72] D. A. Rothschild, W. P. Kopcha, A. Tran, J. Zhang, M. C. Lipke, *Chem. Sci.* **2022**, *13*, 5325–5332.
[73] D. Zhang, R. L. Snider, M. R. Crawley, M. Fang, K. R. Sanchez-Lievanos, S. Ang, T. R. Cook, *Inorg. Chem.* **2024**, *63*, 22532–22541.
[74] S. A. Yao, C. B. Hansen, J. F. Berry, *Polyhedron* **2013**, *58*, 2–6.
[75] K. L. Branch, E. R. Johnson, E. M. Nichols, *ACS Cent. Sci.* **2024**, *10*, 1251–1261.
[76] A. N. Marianov, A. S. Kochubei, T. Roman, O. J. Conquest, C. Stampfl, Y. Jiang, *ACS Catal.* **2021**, *11*, 3715–3729.
[77] A. Lashgari, C. K. Williams, J. L. Glover, Y. Wu, J. Chai, J. "Jimmy" Jiang, *Chem. - Eur. J.* **2020**, *26*, 16774–16781.
[78] E. Laviron, *J. Electroanal. Chem. Interfacial Electrochem.* **1979**, *101*, 19–28.
[79] C. Léger, P. Bertrand, *Chem. Rev.* **2008**, *108*, 2379–2438.
[80] R. G. Agarwal, S. C. Coste, B. D. Groff, A. M. Heuer, H. Noh, G. A. Parada, C. F. Wise, E. M. Nichols, J. J. Warren, J. M. Mayer, *Chem. Rev.* **2022**, *122*, 1–49.
[81] B. D. Baker Cortés, M. Enache, K. Küster, F. Studener, T.-L. Lee, N. Marets, V. Bulach, M. W. Hosseini, M. Stöhr, *Chem. - Eur. J.* **2021**, *27*, 12430.
[82] U. Mazur, K. W. Hipps, *J. Phys. Chem. C.* **2018**, *122*, 22803–22820.
[83] T. Marshall-Roth, N. J. Libretto, A. T. Wrobel, K. J. Anderton, M. L. Pegis, N. D. Ricke, T. Van Voorhis, J. T. Miller, Y. Surendranath, *Nat. Commun.* **2020**, *11*, 5283.
[84] A. J. Bard, L. R. Faulkner, H. S. White, *Electrochemical Methods: Fundamentals and Applications*, Wiley, Oxford, **2002**.
[85] Reported computational structures of **C_{60}/C_{70}@BiCage** (ref. 20) show a different conformation of the cage than revealed by SC-XRD for **$(ZnOH_2)_2$BiCage**•$4PF_6^-$. Re-optimization of **C_{60}/C_{70}@BiCage** at a higher level of theory produced conformations of the host more consistent with the crystallographically determined structure. These new calculations will be disclosed in a seperate report and were provided to reviewers of the present work as confidential supporting information.
[86] S. Goswami, D. Ray, K.-i. Otake, C.-W. Kung, S. J. Garibay, T. Islamoglu, A. Atilgan, Y. Cui, C. J. Cramer, O. K. Farha, J. T. Hupp, *Chem. Sci.* **2018**, *9*, 4477–4482.
[87] Y. Wang, N.-Y. Huang, H.-Y. Wang, X.-W. Zhang, J.-R. Huang, P.-Q. Liao, X.-M. Chen, J.-P. Zhang, *CCS Chem.* **2023**, *5*, 145–151.
[88] D. V. Konarev, S. S. Khasanov, G. Saito, R. N. Lyubovskaya, *Cryst. Growth Des.* **2009**, *9*, 1170–1181.
[89] D. V. Konarev, S. S. Khasanov, M. A. Faraonov, R. N. Lyubovskaya, *CrystEngComm* **2012**, *14*, 4350–4356.
[90] D. R. Evans, N. L. P. Fackler, Z. Xie, C. E. F. Rickard, P. D. W. Boyd, C. A. Reed, *J. Am. Chem. Soc.* **1999**, *121*, 8466–8474.
[91] J. Li, A. Takeuchi, M. Ozawa, X. Li, K. Saigo, K. Kitazawa, *J. Chem. Soc. Chem. Commun.* **1993**, 1784.
[92] C. García-Simón, M. Garcia-Borràs, L. Gómez, T. Parella, S. Osuna, J. Juanhuix, I. Imaz, D. Maspoch, M. Costas, X. Ribas, *Nat. Commun.* **2014**, *5*, 5557.
[93] T. Tsutsui, L. Catti, K. Yoza, M. Yoshizawa, *Chem. Sci.* **2020**, *11*, 8145–8150.
[94] J. Zhang, X. Zheng, R. Jiang, Y. Yu, Y. Li, H. Liu, Q. Li, Z. Shuai, Y. Li, *RSC Adv.* **2014**, *4*, 27389–27392.
[95] A. D. Cardenal, H. J. Park, C. J. Chalker, K. G. Ortiz, D. C. Powers, *Chem. Commun.* **2017**, *53*, 7377–7380.
[96] D. Dubois, G. Moninot, W. Kutner, M. T. Jones, K. M. Kadish, *J. Phys. Chem.* **1992**, *96*, 7137–7145.
[97] C. W. Li, M. W. Kanan, *J. Am. Chem. Soc.* **2012**, *134*, 7231–7234.
[98] M. Lu, M. Zhang, C.-G. Liu, J. Liu, L.-J. Shang, M. Wang, J.-N. Chang, S.-L. Li, Y.-Q. Lan, *Angew. Chem. Int. Ed.* **2021**, *60*, 4864.

[99] H. Gu, G. Shi, L. Zhong, L. Liu, H. Zhang, C. Yang, K. Yu, C. Zhu, J. Li, S. Zhang, C. Chen, Y. Han, S. Li, L. Zhang, *J. Am. Chem. Soc.* **2022**, *144*, 21502–21511.
[100] H. Wu, M. Zeng, X. Zhu, C. Tian, B. Mei, Y. Song, X.-L. Du, Z. Jiang, L. He, C. Xia, S. Dai, *ChemElectroChem* **2018**, *5*, 2717.
[101] Y. Lu, J. Zhang, W. Wei, D.-D. Ma, X.-T. Wu, Q.-L. Zhu, *ACS Appl. Mater. Interfaces* **2020**, *12*, 37986–37992.
[102] N. Morlanés, K. Takanabe, V. Rodionov, *ACS Catal.* **2016**, *6*, 3092–3095.
[103] C. Zhang, P. Gotico, R. Guillot, D. Dragoe, W. Leibl, Z. Halime, A. Aukauloo, *Angew. Chem. Int. Ed.* **2023**, *62*, e202214665.
[104] A. Maurin, M. Robert, *J. Am. Chem. Soc.* **2016**, *138*, 2492–2495.
[105] G. M. Sheldrick, *Acta Crystallogr.* **2015**, *A71*, 3–8.
[106] G. M. Sheldrick, *Acta Crystallogr.* **2015**, *C71*, 3–8.
[107] C. B. Hubschle, G. M. Sheldrick, B. Dittrich, *J. Appl. Cryst.* **2011**, *44*, 1281–1284.
[108] A. L. Spek, *Acta Cryst* **2009**, *D65*, 148–155.
[109] Deposition number 2376804 contains supplementary crystallographic data presented in this paper for **$(ZnOH_2)_2$BiCage•** $4PF_6$. These data are provided free of charge by the joint Cambridge Crystallographic Data Centre and Fachinformationszentrum Karlsruhe Access Structures service.

Manuscript received: February 26, 2025
Revised manuscript received: March 07, 2025
Accepted manuscript online: March 07, 2025
Version of record online: ■■, ■■

Research Article

CO_2 Reduction

D. A. Rothschild, Z. Cao, F. Xie, B. Thomas, T. J. Emge, J. Li, T. Asefa, M. C. Lipke* **e202504630**

Using Host-Guest Chemistry to Examine the Effects of Porosity and Catalyst-Support Interactions on CO_2 Reduction

Porous framework materials and carbon nanotubes are often used to immobilize molecular electrocatalysts. Herein, we employ metalloporphyrin nanocages (M = Fe, Co) and their host-guest complexes with C_{60}/C_{70} as discrete counterparts to these hybrid catalytic materials. The cages achieve high current densities for reducing CO_2 to CO at low overpotentials, and performance can be improved by fullerene guests, suggesting that porosity is not needed for good activity.